Effects of polarization on the de-excitation dark focal spot in STED microscopy

2010 J. Opt. 12 115707

(http://iopscience.iop.org/2040-8986/12/11/115707)

J. Opt. **12** (2010) 115707 (8pp) doi:10.1088/2040-8978/12/11/115707

Effects of polarization on the de-excitation dark focal spot in STED microscopy

Xiang Hao, Cuifang Kuang[1], Tingting Wang and Xu Liu

State Key Laboratory of Modern Optical Instrumentations, Zhejiang University, Hangzhou 310027, People's Republic of China

E-mail: cfkuang@zju.edu.cn

Received 25 July 2010, accepted for publication 13 September 2010
Published 29 October 2010
Online at stacks.iop.org/JOpt/12/115707

Abstract
The size of the dark focal spot directly determines the resolution and stability of stimulated emission depletion (STED) microscopy. This paper investigates the relationship between the size of the dark focal spot and the polarization of the input light beam. The types of fundamental polarization are discussed, their effects on the dark focal spot are compared and the optimized mode for each kind of polarization is proposed. The results of the analysis provide the theoretical basis and reference for designing a STED system.

Keywords: polarization, diffraction theory, fluorescence microscopy

(Some figures in this article are in colour only in the electronic version)

1. Introduction

Stimulated emission depletion (STED) microscopy [1–7], with its capacity to discern details far beyond the diffraction limits, has become a subject of considerable recent interest. Today's STED microscopes are based on confocal ones. The depletion beam, with its doughnut-shaped profile and central intensity equalling zero, eliminates the fluorescence stimulated by the excitation beam and only lets the central light pass [1]. Hence, the crucial problem with a STED system is generating the dark focal spot by using a special arrangement of optical devices including a phase plate [8–10] and aplanatic lens (AL). STED microscopy is able to reach arbitrary resolution in principle. However, apart from optimizing the photo-physics of the dye, the highest resolution will therefore only be reached with an optimal doughnut-shaped distribution that features an intensity of zero in a STED microscope. It is believed that STED can attain higher resolution and stability only when the size of the dark focal spot can be minimized. The general method for achieving this is accretion of the intensity of the input laser beam [11]. However, anyone who employs this approach has to face the risk of irreversible destruction of the samples due to photobleaching, trapping effects, thermal instability or other detrimental effects, especially when the samples are live biological cells. Thus, if the maximal amplitude of the pupil function is limited, phase-only pupil functions deliver the best results [12].

Another potential alternative solution to this conflict is the introduction of diversely polarized input light. Although negligible in low numerical aperture (NA) conditions [13], polarization effects do have a more apparent influence on spot size if the NA is large enough [14]. Early attempts at finding their relationships date back to the mid-20th century. In 1969, Richards [15] explicitly derived the intensity distribution formulae near the focal region on the premise that the input beam was linearly polarized. Radial and azimuthal polarization effects were studied by several authors including Youngworth [16], Kang [17], Boker [18] and others [19–21]. But, to the best of our knowledge, no attention has been paid to the size of the central dark area of a doughnut-shaped focal field.

This paper shows the relationships between the size of the dark focal spot and the polarization of the input light beam. The different types of specific polarization are discussed. Their effects on the dark focal spot are compared and the optimized mode is proposed. In section 2 the theoretical light intensities near the focal spot are derived on the premise of non-aberration conditions. In section 3 profiles of focal spots of differently polarized input light are calculated and discussed. Section 4 contains the conclusion and summary of this work.

[1] Author to whom any correspondence should be addressed.

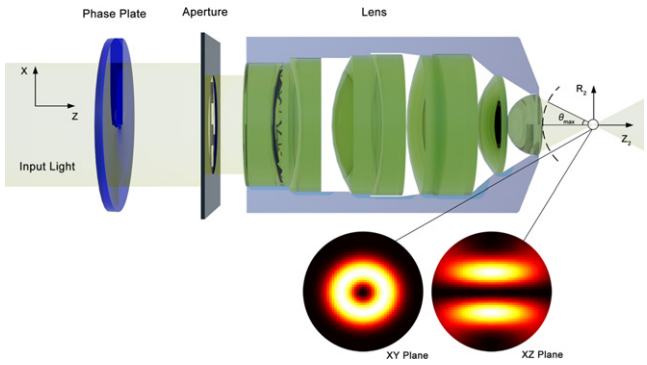

Figure 1. Geometry of the problem. The classic STED microscope structure including the phase plate and the AL.

2. Theory

Figure 1 illustrates the geometry of the problem, in which the classic structure of STED microscopy is adopted. The input light, which has given electrical amplitude and polarization defined by mathematical formulae, propagates through the phase plate and the lens. To simplify the discussion, the focusing is assumed to be done with a high-NA oil-immersion AL having a NA = 1.4; the refractive index of the oil is $n = 1.518$. All aberrations are ignored so that a diffraction-limited axial point image could be expected to locate exactly at the focal spot of the image field. Also, the wavelength of the input light is taken to be unit wavelength while the initial phase is assumed to be the same.

Ignoring aberrations leads to the propagation of light in the image field as a 'focal sphere', with its centre at the focus and with radius equal to the focal length of the AL. Then, according to the geometrical condition

$$h = f \sin\theta \tag{1}$$

where h is the height of the corresponding input ray from the object field, θ is the angle between the ray direction and the optical axis. Furthermore, $0 \leqslant \theta \leqslant \theta_{\max}$, where $\theta_{\max} = \arcsin(\mathrm{NA}/n)$.

The influences on the intensity distribution around the focal spot are four-fold: the polarization condition, the beam shape of the input light, the structure of the lens and the structure of the phase plate. For a high-NA objective lens, by use of vectorial diffraction theory, the electric field vector near the focal spot can be obtained from the generalized Debye integral [15] as

$$\vec{E}(r_2, \varphi_2, z_2) = \mathrm{i}C \int\int_{\Omega} \sin(\theta) \cdot A_1(\theta, \varphi) \cdot A_2(\theta, \varphi) \cdot \begin{bmatrix} p_x \\ p_y \\ p_z \end{bmatrix} \cdot \mathrm{e}^{\mathrm{i}kn(z_2\cos\theta + r_2\sin\theta\cos(\varphi-\varphi_2))}\,\mathrm{d}\theta\,\mathrm{d}\varphi \tag{2}$$

where $\vec{E}(r_2, \varphi_2, z_2)$ is the electric field vector at the point (r_2, φ_2, z_2) expressed in cylindrical coordinates with their origin at the focal point, C is the normalized constant, $A_1(\theta, \varphi)$ is the amplitude function of the input light, $A_2(\theta, \varphi)$ is a 3×3 matrix related to the structure of the imaging lens and $[p_x; p_y; p_z]$ is a matrix unit vector about the polarization of input light.

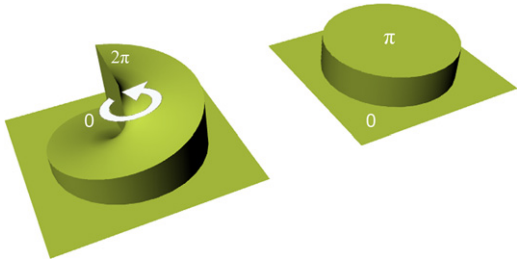

Figure 2. Diagram of the phase plates: vortex 0–2π (left) and circular π (right).

Utilization of the phase plate would cause a phase delay of the input light. An elaborate phase plate design can optimize the energy distribution of the light and generate an unusual focal spot as expected. When phase plate is inserted into the optical microscopy system, equation (2) should be rewritten as

$$\vec{E}(r_2, \varphi_2, z_2) = \mathrm{i}C \int\int_{\Omega} \sin(\theta) \cdot A_1(\theta, \varphi) \cdot A_2(\theta, \varphi) \cdot \begin{bmatrix} p_x \\ p_y \\ p_z \end{bmatrix} \cdot \mathrm{e}^{\mathrm{i}\Delta\alpha(\theta,\varphi)} \mathrm{e}^{\mathrm{i}kn(z_2\cos\theta + r_2\sin\theta\cos(\varphi-\varphi_2))}\,\mathrm{d}\theta\,\mathrm{d}\varphi \tag{3}$$

where $\Delta\alpha(\theta, \varphi)$ is the phase delay parameter.

Considering the most general conditions in STED microscopy, there are limited options for the beam shape of the input light: ideal plane wave or the family of Gaussian beams, such as fundamental Gaussian, Bessel–Gaussian and/or Laguerre–Gaussian. Therefore, the amplitude function $A_1(\theta, \varphi)$ equals 1 or the deformation of the fundamental Gaussian function. Further, $A_2(\theta, \varphi)$ could be expressed as

$$A_2(\theta, \varphi) = a(\theta) \cdot V(\theta, \varphi) \tag{4}$$

where $a(\theta)$ is the apodization factor obtained from energy conservation and geometric considerations [22] and $V(\theta, \varphi)$ is the conversion matrix of the polarization from the object field to the image field. In particular, for the AL [14, 23],

$$a(\theta) = \sqrt{\cos\theta} \tag{5}$$

$$V(\theta, \varphi) = \begin{bmatrix} 1 + (\cos\theta - 1)\cos^2\varphi & (\cos\theta - 1)\cos\varphi\sin\varphi & -\sin\theta\cos\varphi \\ (\cos\theta - 1)\cos\varphi\sin\varphi & 1 + (\cos\theta - 1)\sin^2\varphi & -\sin\theta\sin\varphi \\ \sin\theta\cos\varphi & \sin\theta\sin\varphi & \cos\theta \end{bmatrix}. \tag{6}$$

In the STED system, the function of the phase plate is to generate a doughnut-like focal field with a dark spot at its centre surrounded by high light intensity in all spatial directions. Whether transverse or longitudinal resolution is increased will determine what kind of phase plate is employed: a vortex 0–2π one, a circular π one or both (see figure 2). For a vortex 0–2π phase plate

$$\Delta\alpha = \varphi. \tag{7}$$

For a circular π phase plate

$$\Delta\alpha = 0 \quad (R' \leqslant r \leqslant R) \qquad \Delta\alpha = \pi \quad (0 \leqslant r < R'). \tag{8}$$

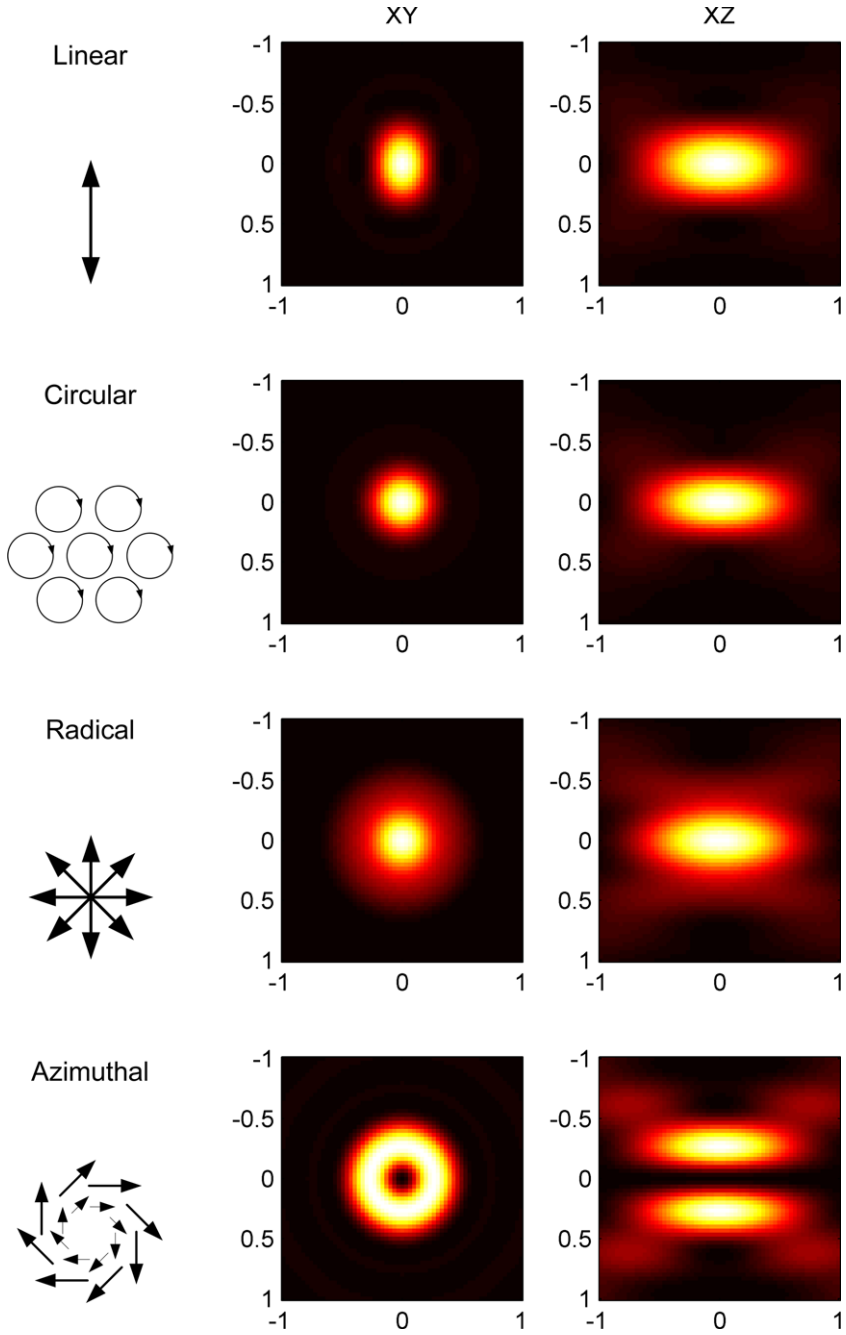

Figure 3. Normalized intensity distribution of focus in an optical system without a phase plate in the horizontal (XY) and longitudinal (XZ) planes. Azimuthally polarized light will generate a doughnut-shaped focal spot in the XY plane, while for other polarized light only a Gaussian-like spot can be expected. Although in such a system these could not be used as the depletion beam, they are still an ideal selection for the excitation beam. Here intensities of 0 and 1 correspond to black and white, respectively. The axis units are in wavelengths.

3. Results and discussion

By using the self-adaptive Simpson's rule [24], numerical integration is done without difficulty. In this section, six classic polarizations, linear (X direction and Y direction), circular (right-handed and left-handed), right-handed ellipse (with X and Y as the long axis), radial and azimuthal ones are under consideration. The calculation results illustrate that the doughnut focal point can be achieved either by the combination of a typical polarized light beam and the phase plate, or only by the light with some complex but well designed polarization. All conditions are shown in table 1.

Without the phase plate, the horizontal doughnut-shaped dark focal spot is still achievable by use of azimuthally polarized light (figure 3).

If the vortex 0–2π phase plate is used, the results of the different polarizations are as given in figure 4.

If the circular π phase plate is used, the results of different polarizations are as given in figure 5.

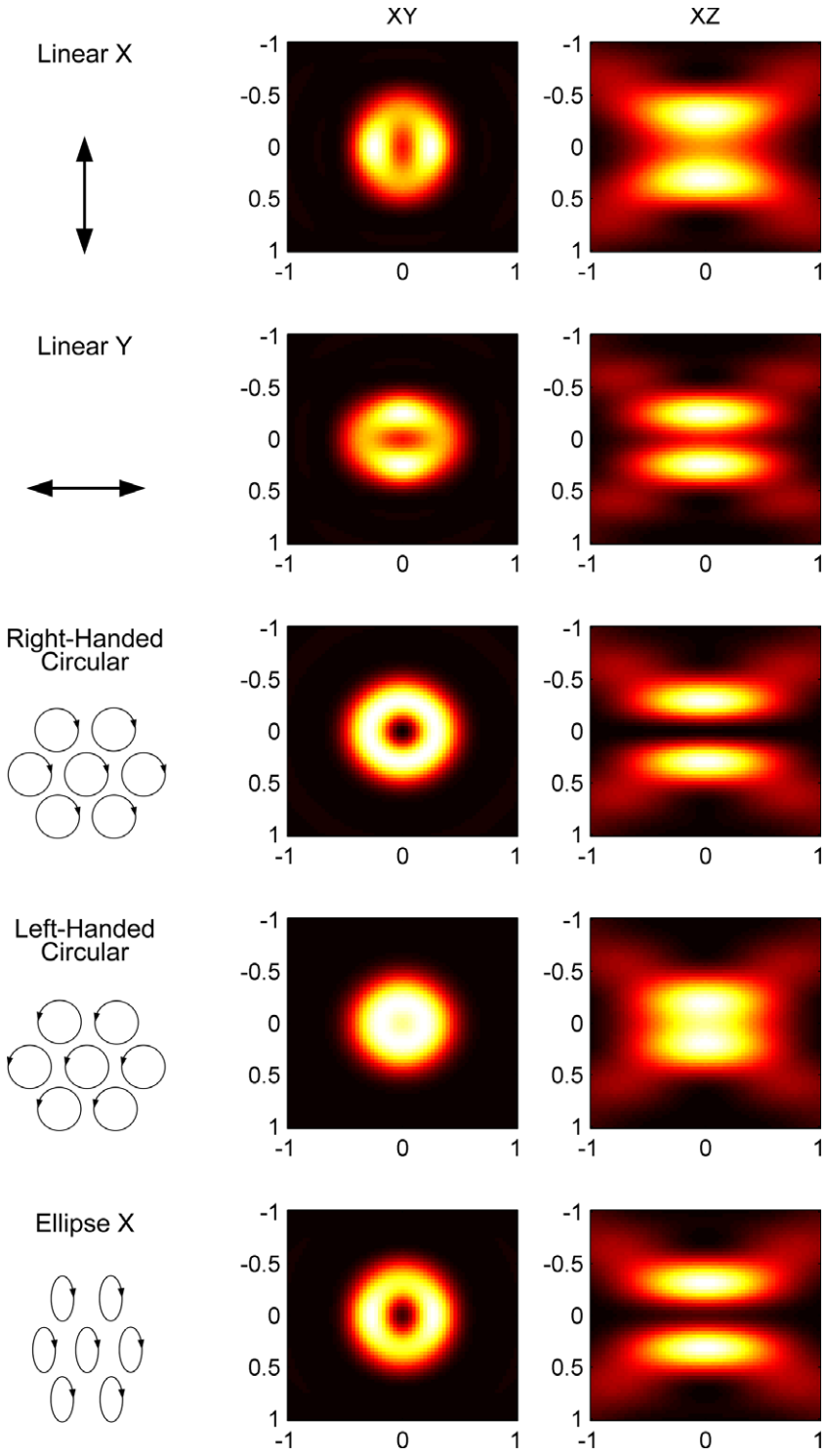

Figure 4. Normalized intensity of polarized light with a vortex 0–2π phase plate at the focal spot in the horizontal (XY) and longitudinal (XZ) planes. Various polarizations are considered: linear (X and Y direction), circular (right-handed and left-handed), right-handed ellipse (with X and Y as the long axis), radial and azimuthal (right-handed and left-handed). Intensities of 0 and 1 correspond to black and white, respectively. The axis units are in wavelengths.

Figures 3–5 shows that colossal distributions of intensity at the focus (XY plane) and through the focus (XZ plane) are produced with the changes in polarization status. Among the six fundamental polarizations, azimuthal polarization is the only one which generates the doughnut-shaped focal spot in the XY plane without any phase plate being inserted into the optical system. By utilizing a vortex 0–2π phase plate, similar results could be expected if the input light is right-handed circular and/or elliptically polarized, while the intensities at the centre of the focal spot are too far from zero when using

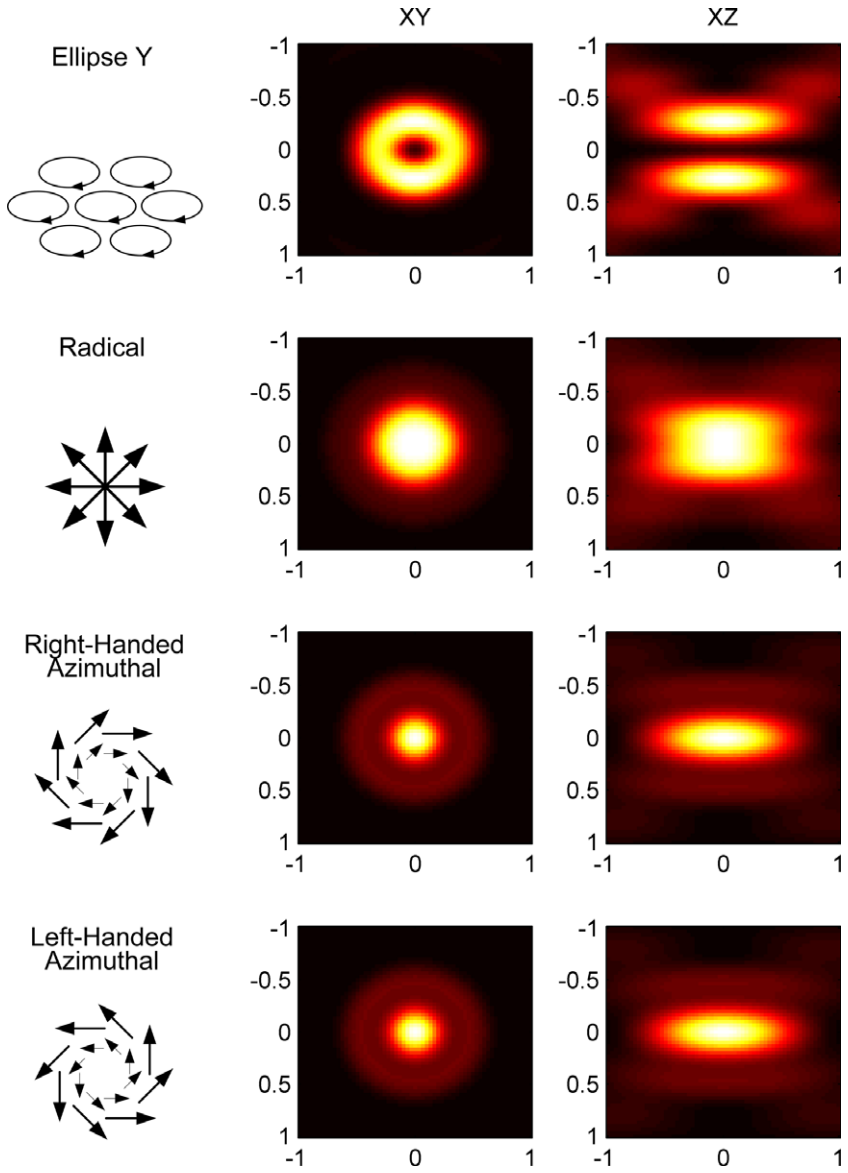

Figure 4. (Continued.)

Table 1. Polarization and corresponding unit vector matrix.

Polarization	Linear X	Linear Y	Right circular	Left circular	Ellipse X	Radial	Azimuthal
$\begin{bmatrix} p_x \\ p_y \\ p_z \end{bmatrix}$	$\begin{bmatrix} 1 \\ 0 \\ 0 \end{bmatrix}$	$\begin{bmatrix} 0 \\ 1 \\ 0 \end{bmatrix}$	$\frac{1}{\sqrt{2}}\begin{bmatrix} 1 \\ \mathrm{i} \\ 0 \end{bmatrix}$	$\frac{1}{\sqrt{2}}\begin{bmatrix} \mathrm{i} \\ 1 \\ 0 \end{bmatrix}$	$\frac{1}{\sqrt{5}}\begin{bmatrix} 2 \\ \mathrm{i} \\ 0 \end{bmatrix}$	$\begin{bmatrix} \cos\theta \\ \sin\theta \\ 0 \end{bmatrix}$	$\begin{bmatrix} -\sin\theta \\ \cos\theta \\ 0 \end{bmatrix}$

linear and/or left-handed circular polarization, although the phenomenon of a doughnut-shaped focal spot indeed exists. If using radial and/or azimuthal polarization, the peak of light intensity would locate accurately at the focal point and only a Gaussian-like focal spot could be detected. Furthermore, in figure 4, the focal point of azimuthally polarized light is sharper that of radially polarized light when they are focused after using a vortex 0–2π phase plate, and even sharper than that of circular polarization without a phase plate. Thus the azimuthal polarized light can be used in a super resolution confocal microscopy system or as excitation light in a STED microscopy system. To our knowledge, this has never been reported in previous works.

The circular π phase plate has the capability of shifting power along the longitudinal direction and generating two intensity peaks at $z_2 \neq 0$. Light with linear, circular and/or elliptical polarization could generate a comparatively better doughnut spot, as shown in figure 5. However, a uniform intensity distribution is not achievable for linear and elliptical polarization in the XY plane. Hence, such polarizations are

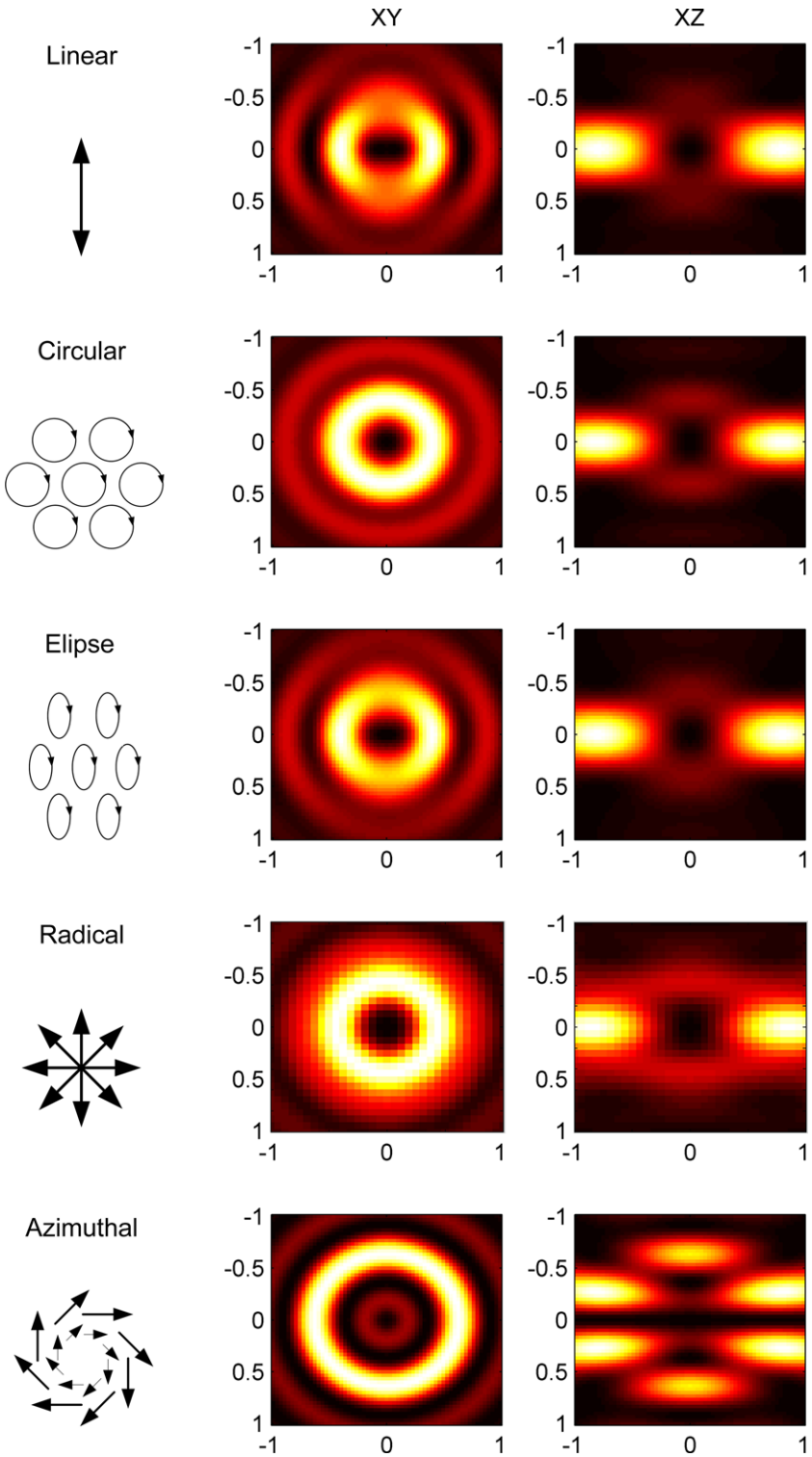

Figure 5. Normalized intensity of polarized light with a circular π phase plate at the focal spot in the horizontal (XY) and longitudinal (XZ) planes. The whole optical system becomes cylindrically symmetrical, so chiral effects of polarization to the spot can be neglected. Here only the results of linear, circular, elliptical, radial and azimuthal polarization are shown. Intensities of 0 and 1 correspond to black and white, respectively. The axis units are in wavelengths.

not suitable for the STED system. On the other hand, radial and azimuthal polarization alone have no practical use in present STED systems because they cannot generate a uniform dark focal spot. But combination with other polarized beams gives the potential to attain better performance, especially if multiple incoherent de-excitation beams are selectable [25]. The circular polarized beam phase-encoded by a vortex 0–2π phase plate, combined with a radial or azimuthal polarized

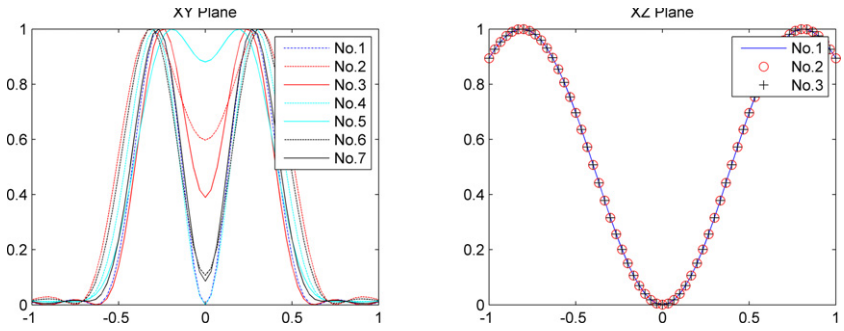

Figure 6. Normalized intensity distribution in the XY plane of a vortex 0–2π phase plate optical system and in the XZ plane of a circular π phase plate optical system. In the XY plane (left graph), azimuthal polarization without a phase plate (no. 1) is shown. When introducing a 0–2π phase plate into the optical system, X-directional linear polarization (no. 2), Y-directional linear polarization (no. 3), right-handed circular polarization (no. 4), left-handed circular polarization (no. 5), elliptical polarization with X as the long axis (no. 6) and with Y as the long axis (no. 7) are also represented. In the XZ plane (right graph), the only effective method for generating a Z-directional doughnut focal spot is by using a circular π phase plate. In this condition, results of linear polarization (no. 1), circular polarization (no. 2) and radial polarization (no. 3) are represented.

beam encoded by a circular 0/π phase plate, could generate a doughnut focal spot in the XY plane with a greater focal depth, as long as over 2.5λ.

Sections of the intensities mentioned above are illustrated in figure 6.

Figure 6 gives a more explicit quantitative analysis of the results. For the XY plane, using azimuthal polarization without any phase plate (no. 1) and right-handed polarization with the vortex 0–2π phase plate (no. 4) is more advantageous than any other polarization status, since the right-handed and azimuthal polarizations can generate perfect 'zero' darkness near the focal spot. The azimuthally polarized input light without any phase plate performs best in the XY plane (the radius of the dark focal spot is about 0.13λ). For the circular π phase plate, results of linear polarization (no. 1), circular polarization (no. 2) and elliptical polarization (no. 3) are almost same in the XZ plane, but linear and elliptical polarization are not uniform in the XY plane. Furthermore, comparing the intensity distribution of a vortex 0–2π phase plate optical system with that of the XZ plane of a circular π phase plate optical system, the effect of the polarization in the latter is relatively smaller than in the former system.

No matter what kind of phase plate is used in the optical system, the only difference between the focal spots generated by circular and elliptical polarization is the uniformity of the intensity distribution of the bright part in the XY plane. The doughnut focal spot always has two intensity peaks in the vertical direction of its long axis if the imported light has elliptical polarization, while doughnut focal spot becomes more even when perfect circular polarization is used. A potential application of this phenomenon is in detecting and optimizing the circular polarization in some particular situations.

An illusion may occur if just the phenomenon in the XY plane of figure 5 is observed; the optical system with a circular π phase plate could break the transverse and longitudinal diffraction limits and achieve the ultimate high resolution because such a system could generate a doughnut focal spot in both the XY and XZ planes if the proper polarization is selected. However, this is difficult under practical experimental condition because the disparity in power levels between the intensity peaks in the XY plane and the XZ plane can be as much as six-fold during simulation calculations. Generally, a single inhibition pattern cannot efficiently cover all polarization components and all directions around an intensity of zero. Thus, in order to achieve 3D dark focal spots, several polarizations of light and phase plates are combined and used in a STED system.

4. Conclusion

The methods introduced here will be an important tool for the efficient design and creation of inhibition fields with multiple intensity zeros when light with different polarizations is used. In this paper, the relationships between size of the dark focal spot and polarization of the input light beam in an aplanatic STED system are represented. Related formulae are explicitly derived, and results are calculated using numerical methods. Four aspects of influence, especially the polarization, are discussed. Their effects on the dark focal spot are compared in detail. In a practical STED system, when considering transverse resolution, input light with azimuthal polarization should be considered. To simplify the generation of typical polarization modes of input light, right-handed polarization with a vortex 0–2π phase plate can be used. Comparatively more options are available when longitudinal resolution is required: right-handed circular and left-handed circular polarization with a circular π phase plate are all possible solutions. In addition, the combination of multiform polarization and multiplex phase plates has the potential capability to attain better performance.

Acknowledgments

This work was financially supported by Zheijiang Provincial Natural Science Foundation of China (No. Y1100408), a grant of the Fundamental Research Funds for the Central Universities (No. 2010QNA5035) and funding from the

State Key Laboratory of Modern Optical Instrumentations (Zhejiang University). The authors thank Dr Yong Liu and Mr Muhammad Yakut Ali for discussions.

References

[1] Hell S W and Wichmann J 1994 Breaking the diffraction resolution limit by stimulated-emission-stimulated-emission-depletion fluorescence microscopy *Opt. Lett.* **19** 780–2
[2] Torok P and Munro P R T 2004 The use of Gauss–Laguerre vector beams in STED microscopy *Opt. Express* **12** 3605–17
[3] Hell S W 2007 Breaking Abbe's barrier: diffraction-unlimited resolution in far-field microscopy *Cytometry* A **71A** 742
[4] Moneron G and Hell S W 2009 Two-photon excitation STED microscopy *Opt. Express* **17** 14567–73
[5] Wildanger D *et al* 2009 A STED microscope aligned by design *Opt. Express* **17** 16100–10
[6] Deng S H *et al* 2010 Effects of primary aberrations on the fluorescence depletion patterns of STED microscopy *Opt. Express* **18** 1657–66
[7] Reuss M, Engelhardt J and Hell S W 2010 Birefringent device converts a standard scanning microscope into a STED microscope that also maps molecular orientation *Opt. Express* **18** 1049–58
[8] Harke B *et al* 2008 Resolution scaling in STED microscopy *Opt. Express* **16** 4154–62
[9] Kuang C F and Wang G R 2010 A novel far-field nanoscopic velocimetry for nanofluidics *Lab Chip* **10** 240–5
[10] Kuang C F, Zhao W and Wang G R 2010 Far-field optical nanoscopy based on continuous wave laser stimulated emission depletion *Rev. Sci. Instrum.* **81** 053709
[11] Hell S W 2003 Toward fluorescence nanoscopy *Nat. Biotechnol.* **21** 1347–55
[12] Keller J, Schonle A and Hell S W 2007 Efficient fluorescence inhibition patterns for RESOLFT microscopy *Opt. Express* **15** 3361–71
[13] Hernandez-Aranda R I and Gutierrez-Vega J C 2008 Focal shift in vector Mathieu–Gauss beams *Opt. Express* **16** 5838–48
[14] Quabis S *et al* 2000 Focusing light to a tighter spot *Opt. Commun.* **179** 1–7
[15] Richards B and Wolf E 1959 Electromagnetic diffraction in optical systems. 2. Structure of the image field in an aplanatic system *Proc. R. Soc.* A **253** 358–79
[16] Youngworth K S and Brown T G 2000 Focusing of high numerical aperture cylindrical-vector beams *Opt. Express* **7** 77–87
[17] Kang H, Jia B H and Gu M 2010 Polarization characterization in the focal volume of high numerical aperture objectives *Opt. Express* **18** 10813–21
[18] Bokor N and Davidson N 2007 A three dimensional dark focal spot uniformly surrounded by light *Opt. Commun.* **279** 229–34
[19] Zhan Q W and Leger J R 2002 Focus shaping using cylindrical vector beams *Opt. Express* **10** 324–31
[20] Cooper I J, Roy M and Sheppard C J R 2005 Focusing of pseudoradial polarized beams *Opt. Express* **13** 1066–71
[21] Lerman G M and Levy U 2008 Effect of radial polarization and apodization on spot size under tight focusing conditions *Opt. Express* **16** 4567–81
[22] Davidson N and Bokor N 2004 High-numerical-aperture focusing of radially polarized doughnut beams with a parabolic mirror and a flat diffractive lens *Opt. Lett.* **29** 1318–20
[23] Zhang Y, Li X and Zhu J 2009 Generation and focusing property with high-numerical aperture lens of ventorial polarized beam *Chin. J. Lasers* **36** 129–33
[24] Atkinson K E and Kendall A 1989 *An Introduction to Numerical Analysis* 2 edn (New York: Wiley)
[25] Kempe M 2010 Microscope with higher resolution and method for increasing same *US Patent Specification* 7709809